High-Quality Metal Oxide Core/Shell Nanowire Arrays on Conductive Substrates for Electrochemical Energy Storage

Xinhui Xia,[†,‡] Jiangping Tu,[†,*] Yongqi Zhang,[†] Xiuli Wang,[†] Changdong Gu,[†] Xin-bing Zhao,[†] and Hong Jin Fan[‡,*]

[†]State Key Laboratory of Silicon Materials and Department of Materials Science and Engineering, Zhejiang University, Hangzhou 310027, People's Republic of China, and [‡]Division of Physics and Applied Physics, School of Physical and Mathematical Sciences, Nanyang Technological University, Singapore 637371

ABSTRACT

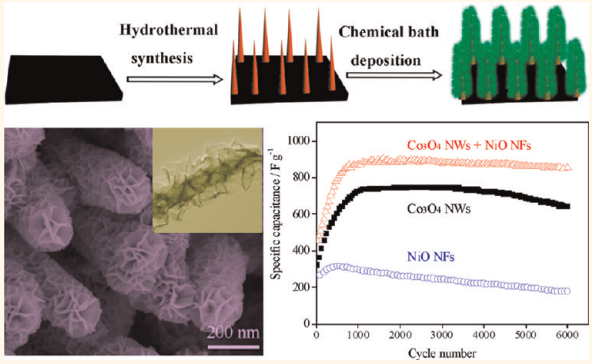

The high performance of a pseudocapacitor electrode relies largely on a scrupulous design of nanoarchitectures and smart hybridization of bespoke active materials. We present a powerful two-step solution-based method for the fabrication of transition metal oxide core/shell nanostructure arrays on various conductive substrates. Demonstrated examples include Co_3O_4 or ZnO nanowire core and NiO nanoflake shells with a hierarchical and porous morphology. The "oriented attachment" and "self-assembly" crystal growth mechanisms are proposed to explain the formation of the NiO nanoflake shell. Supercapacitor electrodes based on the Co_3O_4/NiO nanowire arrays on 3D macroporous nickel foam are thoroughly characterized. The electrodes exhibit a high specific capacitance of 853 F/g at 2 A/g after 6000 cycles and an excellent cycling stability, owing to the unique porous core/shell nanowire array architecture, and a rational combination of two electrochemically active materials. Our growth approach offers a new technique for the design and synthesis of transition metal oxide or hydroxide hierarchical nanoarrays that are promising for electrochemical energy storage, catalysis, and gas sensing applications.

KEYWORDS: core/shell · nanowire arrays · cobalt oxide · nickel oxide · supercapacitor · electrochemical storage

One-dimensional (1D) heterostructured nanomaterials have been of great scientific and technological interests due to their high versatility and applicability as essential components in nanoscale electronics, catalysis, chemical sensing, and energy conversion storage devices.[1−3] Currently, tremendous efforts have been devoted to the rational synthesis of advanced core/shell nanowire heterostructures with fascinating synergetic properties or multifunctionalities offered by the composite nanostructures. Various core/shell nanowire heterostructures such as semiconductor/semiconductor,[4−6] semiconductor/metal,[7] metal/metal oxide,[8−10] metal/metal,[11−13] metal oxide/metal oxide,[14−22] and metal oxide/conductive polymer[23] have been explored, and enhanced properties have been demonstrated. The heterostructured nanowire architecture can make use of the advantages of both components and offer special properties through a reinforcement or modification of each other. Transition metal oxides such as Co_3O_4, NiO, and ZnO are technologically important materials for applications in lithium-ion batteries, gas sensing, catalysis, and electrochromic devices. To meet these applications, it is desirable to integrate these oxides into core/shell nanowire arrays to achieve enhanced electrical, optical, electrochemical, and mechanical properties.

The fabrication of core/shell nanowire arrays with well-defined morphologies and tunable functions still remains a challenge. Progress has been achieved in developing cost-effective and simple methods for controlling nanowire growth as well as creating more complex heterostructures.[24] Core/shell nanowire arrays are generally grown by the catalyst-assisted vapor−liquid−solid mechanism and template-based approaches.[1] However, there is still no simple and high-efficiency method to synthesize transition metal oxide or hydroxide core/shell nanostructure arrays with precise structure control, even though a few successful strategies (electrodeposition,[16] oxidation,[18] wet-chemical methods based on sacrificial templates,[19] and physical technique such as sputtering and pulsed laser deposition[15]) have been reported.

* Address correspondence to fanhj@ntu.edu.sg, tujp@zju.edu.cn.

Received for review April 3, 2012 and accepted April 30, 2012.

Published online May 01, 2012
10.1021/nn301454q

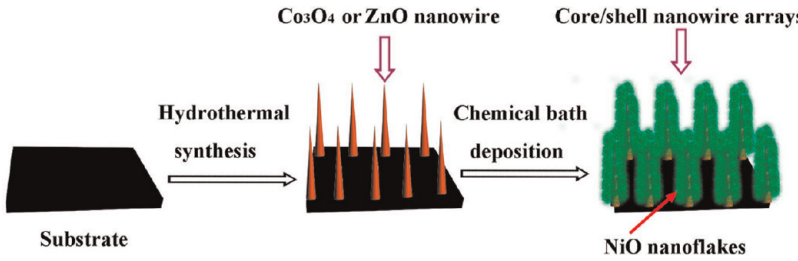

Figure 1. Schematic illustration of the two-step synthesis of metal oxide core/shell nanowire arrays directly on various substrates.

Transition metal oxides/hydroxides store electrochemical energy by revesible surface faradaic (redox) reactions. MnO_2, NiO, $Ni(OH)_2$, CoO_x, and their compounds are under recent focus in the design of high-energy-density pseudocapacitor electrodes.[19,23,25−31] To meet the requirement of higher specific capacitance and structural stability, one promising route is to have scrupulous design of nanoarchitectures and smart hybridization of bespoke pseudocapacitive oxides.

In the present work, we present a simple but powerful two-step solution method to synthesize transition metal oxide core/shell nanoarrays on a variety of substrates including transparent conducting glass, nickel foil, and nickel foam. The superior supercapacitor performance of electrodes based on Co_3O_4/NiO nanowire arrays grown on nickel foam will be demonstrated, followed by discussion on the enhancement mechanism. Due to the unique properties of these core/shell nanoarrays, such as high surface areas, crystallinity, and good conductivity and direct growth on conductive substrates, they have potential applications in lithium-ion batteries, chemical sensing, electrochemical or photocatalysis, field emission, electrochromic devices, and energy conversion storage.

RESULTS AND DISCUSSION

Figure 1 illustrates the two-step synthesis of the Co_3O_4/NiO and ZnO/NiO core/shell nanowire arrays by combining hydrothermal synthesis and chemical bath deposition methods. The hydrothermally synthesized Co_3O_4 or ZnO nanowire arrays serve as the backbone for the subsequent deposition of NiO nanoflakes. The resulting core/shell nanowire arrays can be realized on a variety of conductive substrates including fluorine-doped tin oxide glass (FTO), nickel foil, and nickel foam (see Supporting Information, Figures S1 and S2). There is no apparent difference in the array morphology on different substrates, indicating the generality of this two-step solution method. The morphologies of the Co_3O_4 nanowires and final Co_3O_4/NiO core/shell nanowires on FTO substrate are shown in Figure 2. The Co_3O_4 nanowires have an average diameter of 70 nm and length up to around 10 μm. After chemical bath deposition, the Co_3O_4 nanowires are decorated with NiO nanoflakes that are ~10 nm thick. The NiO nanoflake shells are interconnected but still do not fully cover the entire Co_3O_4 core. Cross-sectional SEM images of the core/shell nanowires (Figure 2e,f) confirm the unique core/shell heterostructure.

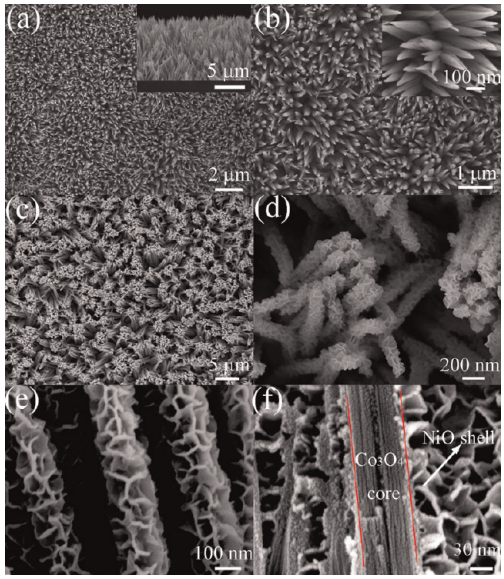

Figure 2. SEM images of (a,b) Co_3O_4 nanowire arrays and (c,d) Co_3O_4/NiO core/shell nanowire arrays grown on FTO substrate. (e,f) Enlarged view of the core/shell nanowires showing the flake morphology of the NiO.

The Co_3O_4 core nanowire and NiO shell nanoflake can be easily distinguished from the TEM images (Figure 3). The Co_3O_4 core nanowires are highly porous, composed of nanocrystallites of 10−20 nm in size and pores of 2−4 nm. However, the nanowires are crystalline in whole, as revealed by the SAED pattern, which implies that nanocrystallites are oriented in order (Figure 3a,b and Figure S3 in Supporting Information). The as-prepared mesoporous Co_3O_4 nanowire is quite different from ammonia-evaporation-induced mesoporous Co_3O_4 nanowires, which show a quasi-single-crystalline hollow structure.[26,27] The nanoflake shell (Figure 3e) shows a polycrystalline SAED pattern corresponding to the cubic NiO phase. This core/shell heterostructure is also supported by energy-dispersive X-ray spectroscopy (EDS) elemental mapping of Co and Ni (Figure 3g). X-ray diffraction (XRD) pattern shows that the core/shell nanowire arrays contain spinel Co_3O_4 phase (JCPDS 42-1467) and cubic NiO phase (JCPDS 4-0835) (Figure S4), which is also supported by

Fourier transform infrared (FTIR) results (Figure S5). Because of the porous core and flake shell, the Co_3O_4/NiO nanowire arrays exhibit a quite large surface area of 415 m^2/g (Figure S6). The NiO shell thickness and Co_3O_4 nanowire length can be easily controlled by changing the reaction time. This provides us with the ability to tune electrochemical properties of the core/shell nanowire arrays.

Given the wide application of hydrothermal growth and chemical bath deposition for metal hydroxides and oxides, the synthesis protocol presented here is robust and efficient and can be extended to the fabrication of other core/shell nanowire arrays, such as ZnO/NiO core/shell nanowire arrays (see Figure 4). Herein, the hydrothermally synthesized ZnO nanowires are single-crystalline solid rods with an average diameter of 100 nm. The same chemical bath deposition of NiO results in ZnO/NiO arrays that exhibit similar core/shell heterostructure with the above Co_3O_4/NiO arrays. Using the same methodology, we have recently obtained TiO_2/NiO core/shell nanoarrays (data not shown). This implies that the chemical bath deposition of NiO is not restricted by the nanowire scaffold.

The growth mechanism of the shell structure is proposed as follows (also shown schematically in Figure 5). Most likely, it is due to the "oriented attachment" and "self-assembly" processes,[28,32,33] which involve a spontaneous self-organization of adjacent particles so that they share a common crystallographic orientation, followed by joining of these particles at a planar interface. The process is particularly relevant in the nanocrystalline regime, where bonding between the particles reduces overall energy by removing surface energy associated with unsatisfied bonds.[28,34] In our case, the Co_3O_4 or ZnO nanowire acts as the backbone to guide the Ni-based hydroxide preferential deposition. Heterogeneous nucleation occurs after supersaturated solution with numerous Ni-based hydroxide mesocrystals is formed. Then Ni-based hydroxide mesocrystals attach to the surface of Co_3O_4 or ZnO nanowires, forming active nucleation centers by reducing the surface energy. These active sites would minimize the interfacial energy barrier for the subsequent growth of Ni-based hydroxide.[35] Finally, these Ni-based hydroxide mesocrystals self-assemble, leading

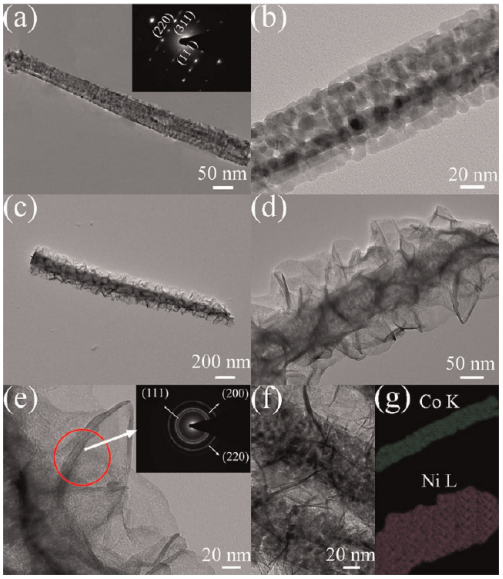

Figure 3. TEM characterization of (a,b) Co_3O_4 nanowire and (c–f) Co_3O_4/NiO core/shell nanowire. (e) NiO nanoflake shell (inset: SAED pattern). (f) Porous nature of the Co_3O_4 core nanowire. (g) EDS maps of Co and Ni.

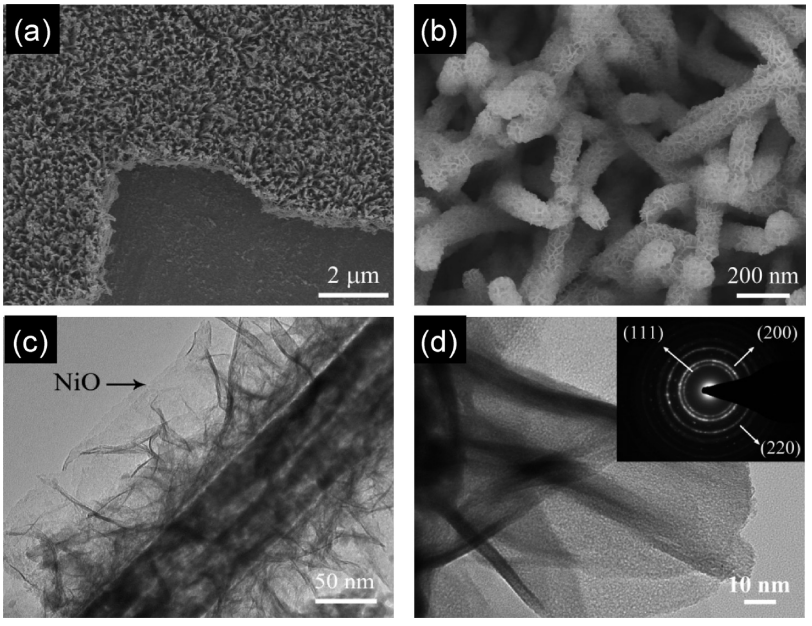

Figure 4. ZnO/NiO core/shell nanowire arrays grown on FTO using similar growth method. (a,b) SEM images, (c,d) TEM images (SAED pattern in inset).

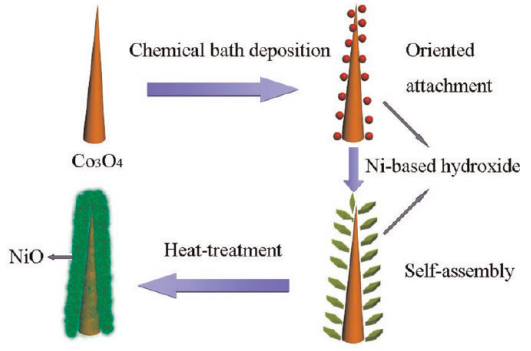

Figure 5. Schematic illustration of the growth mechanism of the NiO nanoflakes on Co_3O_4 or ZnO nanowire backbone. Red balls represent Ni-based hydroxide mesocrystals in the aqueous solution. Green rhombuses are self-assembled Ni-based hydroxide nanoflakes.

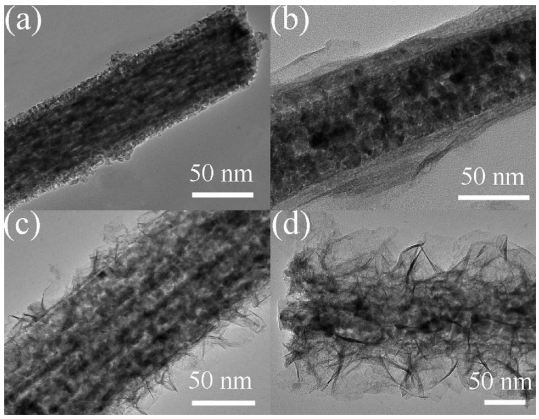

Figure 6. TEM images of the nanostructure obtained after chemical bath deposition for different times, showing the morphology evolution of the core/shell nanowires: (a) 2 min; (b) 4 min; (c) 6 min; (d) 8 min.

to the formation of the quasi-2D flake structure. The above hypothesis is supported by inspecting the morphologies at different growth stages by controlling the time (Figure 6). One can see that nanoparticles start to attach to the surface of the nanowire at the early stage (deposition for 2 min, Figure 6a). As the deposition proceeds, these nanoparticles self-assemble to form large nanoflakes (Figure 6b,c) and finally produce the interesting core/shell heterostructured nanowires (Figure 6d). It is noteworthy that potassium persulfate here plays an important role in the formation of the nanoflake shell. Potassium persulfate acts as an oxidant to drive the whole reaction and facilitate the heterogeneous nucleation in the supersaturated solution. Without potassium persulfate, no nanoflake shell will be formed on the Co_3O_4 nanowire.

We now study the supercapacitor performance of the Co_3O_4/NiO core/shell nanowire arrays for their potential application in electrochemical energy storage. We choose the results of samples grown on nickel foam for discussion because the 3D macroporous nickel form is a superior substrate to Ni foil or FTO (see more discussion on this in Supporting Information). Results are presented in Figure 7 to demonstrate noticeable pseudocapacitive properties. The Co_3O_4/NiO core/shell nanowire arrays present a lower charge plateau and higher discharge plateau (Figure 7a), indicating their enhanced electrochemical reactivity and lower polarization, confirmed by cyclic voltammetry (CV) analysis (Figure 7b). For the individual Co_3O_4 nanowire arrays (see SEM images in Figure S7),[36] two typical redox couples characteristic of Co_3O_4 are observed in the CV curve. The first redox couple A_1/C_1 corresponds to the conversion between CoOOH and Co_3O_4 as follows.[29,37]

$$Co_3O_4 + OH^- + H_2O \leftrightarrow 3CoOOH + e^- \quad (1)$$

The second redox couple A_2/C_2 is attributed to the change between CoOOH and CoO_2, represented by the following reaction:[29,37]

$$CoOOH + OH^- \leftrightarrow CoO_2 + H_2O + e^- \quad (2)$$

For the individual NiO nanoflake arrays (see SEM images in Figure S7), one redox couple N_1/N_2 is observed, represented by the following electrochemical reaction:[38]

$$NiO + OH^- \leftrightarrow NiOOH + e^- \quad (3)$$

For the Co_3O_4/NiO core/shell nanowire arrays, only one oxidation peak P_1 is observed in the anodic process and three reduction peaks P_2, P_3, and P_4 are noticed in the cathodic process. It is justified that the oxidation peak P_1 is an integrated peak of A_1, A_2, and N_1. The reduction peaks P_2, P_3, and P_4 correspond to peaks C_2, C_1, and N_2. Therefore, all of the redox peaks from both Co_3O_4 and NiO are presented. Obviously, the peak currents of the core/shell nanowire arrays are much higher than the single components, indicating that the core/shell nanowire arrays have higher electrochemical reaction activity. Electrochemical impedance spectroscopy (EIS) results (Figure S8) show that the Co_3O_4/NiO core/shell arrays have the lowest charge transfer resistance and ion diffusion resistance, which are both beneficial to the rate capability.

The specific capacitances at various discharge current densities for the three array electrodes without activation are calculated and shown Figure 7c (see their corresponding discharge curves in Figure S9). In our experiment, all specific capacitances are calculated by subtracting the discharge time of nickel foam and reducing the substrate effect to the lowest level (Figure S11). The Co_3O_4/NiO core/shell nanowire arrays exhibit evidently higher specific capacitances and better rate capability than the single components; 85% of capacitance is maintained (from 452 to 384 F/g) for the Co_3O_4/NiO core/shell nanowire arrays when the charge/discharge rate changes from 2 to 40 A/g, much higher than those for the Co_3O_4 nanowire arrays (76.7%) and NiO nanoflake arrays (66.6%). Meanwhile, the discharge areal capacitance of the Co_3O_4/NiO core/shell

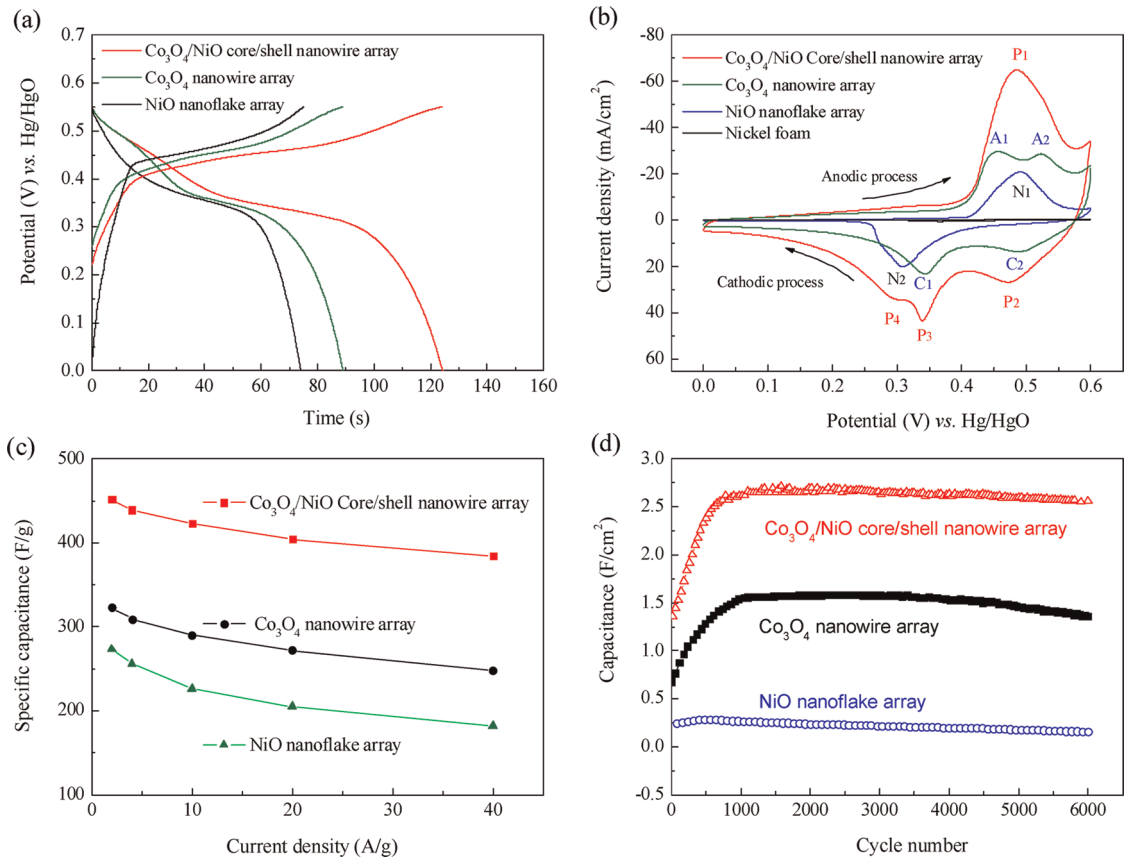

Figure 7. Electrochemical characterization of three array electrodes grown on nickel foam. (a) Charge/discharge curves at 2 A/g at the 10th cycle. (b) CV curves at a scanning rate of 5 mV/s at the 10th cycle. (c) Specific capacitances at different current densities. (d) Cycling performances at 2 A/g.

nanowire arrays is measured to be 1.35 F/cm^2, which is about 2 and 5 times larger than the Co_3O_4 nanowire arrays (0.68 F/cm^2) and NiO nanoflake arrays (0.25 F/cm^2), respectively.

The enhancement in the supercapacitor performance of the core/shell nanowire arrays can also be manifested by their excellent cycling stability and good capacitance retention (Figure 7d). The cycling life of these array electrodes essentially consists of three processes: an activation period, steady state, and a degradation period. In our case, the capacitance increase of the Co_3O_4/NiO electrode in the activation period (1−1000 cycles) is quite large. Generally, only a fraction of material is active during the first cycles, while the rest is not activated. As the electrolyte gradually penetrates into the Co_3O_4/NiO core/shell nanowires, more and more of the core/shell nanowires become activated and contribute to the increase of capacitance. The core/shell nanowire arrays show an areal capacitance of 2.56 F/cm^2 after 6000 cycles and keeps 95.1% of the highest value, much higher than those of the Co_3O_4 nanowire arrays (1.36 F/cm^2 with 85.5%) and NiO nanoflake arrays (0.16 F/cm^2 with 56.7%). Similar result can also been obtained by comparing the specific capacitances after 6000 cycles (see Figure S10). A high specific capacitance of 853 F/g is achieved at 2 A/g for the core/shell nanowire arrays, compared to 642 F/g of the Co_3O_4 nanowire arrays and 178 F/g for the NiO nanoflake arrays.

It is known that the substrate has a nontrivial influence on the electrochemical performance. To check the substrate effect, we further investigated the pseudocapacitive behavior of the Co_3O_4/NiO core/shell nanowire arrays grown on the FTO substrate (data presented in Figure S12). Different from the nanowire arrays on nickel foam, here only one redox couple is observed in the CV curve. The signal of the FTO substrate is negligible. The pseudocapacitance values are also much lower than those on the nickel substrate. Particularly, the high-rate capability on the FTO substrate is quite unsatisfactory. Generally, the active material deposited on 3D porous substrates (such as nickel foam) shows better electrochemical performance than their counterparts on the flat substrate, due to the fact that the 3D porous substrates provide higher active surface area and inner space for fast ion/electron transfer and higher energy conversion efficiency.

The enhanced supercapacitor performance of the core/shell nanostructure arrays can be ascribed to the unique architecture including the porous Co_3O_4 core nanowire, NiO nanoflake shell, and ordered array

configuration. *First*, the porous core/shell array configuration enables the full exposure of both active materials to the electrolyte and thus enhances ion and electron diffusion.[39,40] The NiO nanoflake shells are well separated and construct a porous layer surrounding the Co_3O_4 nanowire core, making both the shell and core fully accessible to the electrolyte. Meanwhile, the highly porous and crystalline Co_3O_4 nanostructures are also electrochemically active, as previously demonstrated.[26,27,29] *Second*, the array structure ensures good mechanical adhesion and electrical connection to the current collector and, therefore, avoids the use of polymer binders and conducting additives. In our case, the sheet resistance for the hydrothermally synthesized porous Co_3O_4 nanowire array and chemical-bath-deposited NiO film is about 40 and 1500 Ω/square, respectively, measured by four points probe technique. *Lastly*, the core/shell configuration has a super strong mechanical stability. The structure of the core/shell nanowire arrays after 6000 cycles still remains intact (see SEM image in Figure S13). In this respect, it is possible that the Co_3O_4 core and flexible NiO shell synergistically prevent the whole nanowires from significant collapse and disassembly during the redox reactions with harsh and frequent phase variations.

Finally, to further demonstrate the versatility of our fabrication method, we also obtained $Co_3O_4/Co(OH)_2$ core/shell nanowire arrays by electrochemical deposition of $Co(OH)_2$ nanoflakes on the same Co_3O_4 nanowire array. This also serves a check if the conductivity of the porous Co_3O_4 nanowire array is good enough as a conductive connection. SEM images of the obtained nanotree-like array are presented in Figure S14. The high success of electrochemial depostion strongly indicates that the Co_3O_4 nanowires have a good electrical conductivity as well as physical contact to the nickel foam.

CONCLUSION

We have presented a facile and high-efficiency, solution-based method for the direct growth of Co_3O_4/NiO and ZnO/NiO core/shell nanowire arrays on various conductive substrates. In this hierarchical structure, the nanowire core is coated with a shell of nanoflakes with a porous morphology. On the basis of control experiments for the Co_3O_4/NiO arrays, a plausible growth mechanism is proposed which involves self-assembly and oriented attachment of nancrystallites. The synthesis route presented here is robust and may be extended to fabricating other core/shell nanowire arrays for various applications in electrochemical energy storage and optical devices. The Co_3O_4/NiO core/shell nanowire arrays grown on the nickel foam exhibit excellent supercapacitor performance with high specific capacitance and good cycling stability, making it one of the best electrode materials for high-performance supercapacitors. The enhanced electrochemical properties can be atributed to the unique porous and conductive, core/shell, and array architecture.

METHODS

Preparation of Co_3O_4/NiO Core/Shell Nanowire Arrays. First, self-supported Co_3O_4 nanowire arrays were prepared by a facile hydrothermal synthesis method. The solution was prepared by dissolving 5 mmol of $Co(NO_3)_2$, 10 mmol NH_4F, and 25 mmol of $CO(NH_2)_2$ in 70 mL of distilled water. Then this resulting solution was transferred into Teflon-lined stainless steel autoclave linears. Various substrates (2×6 cm^2 in sizes) such as FTO glass, nickel foil, and nickel foam were immersed into the reaction solution. Top sides of the substrates were uniformly coated with a polytetrafluoroethylene tape to prevent the solution contamination. The linear was sealed in a stainless steel autoclave and maintained at 120 °C for 5 h and then cooled to room temperature. The samples were collected and rinsed with distilled water several times. Finally, the samples were annealed at 350 °C in normal purity argon for 2 h. The chemical reactions involved in the preparation process of Co_3O_4 nanowire arrays can be illustrated as follows:[27,36]

$$Co^{2+} + xF^- \rightarrow [CoF_x]^{(x-2)-} \quad (4)$$

$$H_2NCONH_2 + H_2O \rightarrow 2NH_3 + CO_2 \quad (5)$$

$$CO_2 + H_2O \rightarrow CO_3^{2-} + 2H^+ \quad (6)$$

$$NH_3 \cdot H_2O \rightarrow NH_4^+ + OH^- \quad (7)$$

$$[CoF_x]^{(x-2)-} + 0.5(2-y)CO_3^{2-} + yOH^- + nH_2O \rightarrow Co(OH)_y(CO_3)_{0.5(2-y)} \cdot nH_2O + xF^- \quad (8)$$

$$Co(OH)_y(CO_3)_{0.5(2-y)} \cdot nH_2O + \frac{1}{2}O_2 \xrightarrow{\text{Annealing}} Co_3O_4 + (3n + 1.5y)H_2O + 1.5(2-y)CO_2 \quad (9)$$

Then, the self-supported Co_3O_4 nanowire arrays were used as the scaffold for NiO nanoflake growth in a simple chemical bath. Co_3O_4 nanowire arrays grown on the different substrates (masked with polyimide tape to prevent deposition on the back sides) were placed vertically in a 250 mL Pyrex beaker. Solution for chemical bath deposition (CBD) was prepared by adding 20 mL of aqueous ammonia (25−28%) to the mixture of 100 mL of 1 M nickel sulfate and 80 mL of 0.25 M potassium. The reactions for chemical bath deposition are represented as follows:[35]

$$[Ni(H_2O)_{6-x}(NH_3)_x]^{2+} + 2OH^- \rightarrow Ni(OH)_2 + (6-x)H_2O + xNH_3 \quad (10)$$

$$2Ni(OH)_2 + S_2O_8^{2-} \rightarrow 2NiOOH + 2SO_4^{2-} + 2H^+ \quad (11)$$

Immersing into the CBD solution for 8 min at 20 °C, the substrates were taken off and rinsed with distilled water. The samples were annealed at 350 °C in argon for 1.5 h. The thickness of the Co_3O_4/NiO core/shell nanowire arrays was approximately 10 μm. It is noted that the potassium persulfate acts as an oxidant to drive the whole reaction; without it, no formation of nanoflakes is observed. As a control sample, self-supported Co_3O_4 nanowire arrays and NiO nanoflake arrays on nickel foam were prepared using the same methods as described above.

Preparation of ZnO/NiO Core/Shell Nanowire Arrays. To facilitate the nucleation of ZnO nanowire growth, a 5 nm thick ZnO thin film

was first deposited on the FTO substrate by sputtering. The hydrothermal reaction solution for ZnO nanorod array fabrication was prepared by mixing 0.05 M zinc acetate and 0.05 M hexamethylenetetramine ($C_6H_{12}N_4$). Then the homogeneous solution was transferred into Teflon-lined stainless steel autoclave linears and heated to 90 °C for 5 h inside a conventional laboratory oven. Subsequently, the sample was rinsed with distilled water. Then the self-supported ZnO nanowire arrays were used as the scaffold for NiO nanoflake growth in a simple chemical bath as mentioned above leading to the formation of ZnO/NiO core/shell nanowire arrays.

Characterization of Co_3O_4/NiO Core/Shell Nanowire Arrays. The samples were characterized by X-ray diffraction (XRD, RIGAKU D/Max-2550 with Cu Kα radiation), field emission scanning electron microscopy (FESEM, FEI SIRION), high-resolution transmission electron microscopy (HRTEM, JEOL JEM-2010F), and Fourier transform infrared (FTIR) measurements (Perkin-Elmer System 2000 FTIR interferometer). The surface area of the film that scratched from the substrate was determined by BET measurements using a NOVA-1000e surface area analyzer.

Electrochemical Measurements. The electrochemical measurements were carried out in a three-electrode electrochemical cell containing 2 M KOH aqueous solution as the electrolyte. The core/shell nanowire arrays were used as the working electrode. Cyclic voltammetry (CV) measurements and electrochemical impedance spectroscopy (EIS) tests were performed on a CHI660c electrochemical workstation (Chenhua, Shanghai). EIS tests were made with a superimposed 5 mV sinusoidal voltage in the frequency range of 100 kHz−0.01 Hz. CV measurements were carried out at a scanning rate of 5 mV/s between 0 and 0.6 V at 25 °C, core/shell nanowire arrays (≈3 × 7 cm^2, Co_3O_4 mass ≈ 2.1 mg/cm^2, NiO mass ≈ 0.9 mg/cm^2) as the working electrode, Hg/HgO as the reference electrode, and a Pt foil as the counter electrode. The galvanostatic charge/discharge tests were conducted on a LAND battery program-control test system. The core/shell nanowire array electrodes, together with a nickel mesh counter electrode and a Hg/HgO reference electrode, were tested in a three-compartment system. The specific capacitance is calculated according to the following equation:

$$C = \frac{I\Delta t}{M\Delta V} \tag{12}$$

where C (F/g) was specific capacitance, I (mA) represented discharge current, and M (mg), ΔV (V), and Δt (s) designated mass of active materials, potential drop during discharge, and total discharge time, respectively.

Conflict of Interest: The authors declare no competing financial interest.

Acknowledgment. The authors would like to acknowledge financial support from China Postdoctoral Science Foundation (Grant No. 20100481401) and Zhejiang Province Education Department Scientific Research Project (Y201119640).

Supporting Information Available: Fourteen supporting figures. Photographs of Co_3O_4/NiO core/shell nanowire arrays grown on FTO glass, nickel foam, and nickel foil substrates (Figure S1); SEM images of Co_3O_4/NiO core/shell nanowire arrays on nickel foam and nickel foil substrates (Figure S2); TEM-HRTEM images of the Co_3O_4 nanowire (Figure S3); XRD patterns of (A) Co_3O_4/NiO core/shell nanowire array (Figure S4); FTIR spectra of Co_3O_4/NiO core/shell nanowire (Figure S5); BET measurement of Co_3O_4/NiO core/shell nanowire arrays (Figure S6); SEM images of the Co_3O_4 nanowire arrays and NiO nanoflake arrays grown on nickel foam (Figure S7); EIS plots of three array electrodes with 100% depth of discharge at the 10th cycle (Figure S8); discharge curves of Co_3O_4/NiO core/shell nanowire arrays, Co_3O_4 nanowire arrays, and NiO nanoflake arrays grown on nickel foam at different current densities without activation (Figure S9); charge/discharge curves for the three array electrodes at the charge/discharge current density at the 6000th cycle and cycling performances of specific capacitances for the three array electrodes (Figure S10); CV curve and cycling performance of discharge electric quantity of the nickel foam (Figure S11); CV behavior and discharge curves of the Co_3O_4/NiO core/shell nanowire arrays grown on the FTO substrate (Figure S12); SEM images of the Co_3O_4/$Co(OH)_2$ core/shell nanowire arrays (Figure S13); SEM image of Co_3O_4/NiO core/shell nanowire array after 6000 cycles (Figure S14). This material is available free of charge *via* the Internet at http://pubs.acs.org.

REFERENCES AND NOTES

1. Agarwal, R. Heterointerfaces in Semiconductor Nanowires. *Small* **2008**, *4*, 1872–1893.
2. Law, M.; Goldberger, J.; Yang, P. D. Semiconductor Nanowires and Nanotubes. *Annu. Rev. Mater. Res.* **2004**, *34*, 83–122.
3. Pan, H.; Feng, Y. P. Semiconductor Nanowires and Nanotubes: Effects of Size and Surface-to-Volume Ratio. *ACS Nano* **2008**, *2*, 2410–2414.
4. Ben-Ishai, M.; Patolsky, F. A Route to High-Quality Crystalline Coaxial Core/Multishell Ge@Si(GeSi)$_n$ and Si@(GeSi)$_n$ Nanowire Heterostructures. *Adv. Mater.* **2010**, *22*, 902–906.
5. Goebl, J. A.; Black, R. W.; Puthussery, J.; Giblin, J.; Kosel, T. H.; Kuno, M. Solution-Based II−VI Core/Shell Nanowire Heterostructures. *J. Am. Chem. Soc.* **2008**, *130*, 14822–14833.
6. Lauhon, L. J.; Gudiksen, M. S.; Wang, C. L.; Lieber, C. M. Epitaxial Core−Shell and Core−Multishell Nanowire Heterostructures. *Nature* **2002**, *420*, 57–61.
7. Wu, Y.; Xiang, J.; Yang, C.; Lu, W.; Lieber, C. M. Single-Crystal Metallic Nanowires and Metal/Semiconductor Nanowire Heterostructures. *Nature* **2004**, *430*, 61–65.
8. Keng, P. Y.; Bull, M. M.; Shim, I. B.; Nebesny, K. G.; Armstrong, N. R.; Sung, Y.; Char, K.; Pyun, J. Colloidal Polymerization of Polymer-Coated Ferromagnetic Cobalt Nanoparticles into Pt-Co_3O_4 Nanowires. *Chem. Mater.* **2011**, *23*, 1120–1129.
9. Kim, B. Y.; Shim, I. B.; Araci, Z. O.; Saavedra, S. S.; Monti, O. L. A.; Armstrong, N. R.; Sahoo, R.; Srivastava, D. N.; Pyun, J. Synthesis and Colloidal Polymerization of Ferromagnetic Au-Co Nanoparticles into Au-Co_3O_4 Nanowires. *J. Am. Chem. Soc.* **2010**, *132*, 3234–3235.
10. Li, L.; Yang, Y. W.; Li, G. H.; Zhang, L. D. Conversion of a Bi Nanowire Array to an Array of Bi-Bi_2O_3 Core−Shell Nanowires and Bi_2O_3 Nanotubes. *Small* **2006**, *2*, 548–553.
11. Koenigsmann, C.; Santulli, A. C.; Gong, K. P.; Vukmirovic, M. B.; Zhou, W. P.; Sutter, E.; Wong, S. S.; Adzic, R. R. Enhanced Electrocatalytic Performance of Processed, Ultrathin, Supported Pd−Pt Core−Shell Nanowire Catalysts for the Oxygen Reduction Reaction. *J. Am. Chem. Soc.* **2011**, *133*, 9783–9795.
12. Sun, Y. G.; Tao, Z. L.; Chen, J.; Herricks, T.; Xia, Y. N. Ag Nanowires Coated with Ag/Pd Alloy Sheaths and Their Use as Substrates for Reversible Absorption and Desorption of Hydrogen. *J. Am. Chem. Soc.* **2004**, *126*, 5940–5941.
13. Zhang, G. Q.; Wang, W.; Li, X. G. Enhanced Thermoelectric Properties of Core/Shell Heterostructure Nanowire Composites. *Adv. Mater.* **2008**, *20*, 3654–3656.
14. Chueh, Y. L.; Chou, L. J.; Wang, Z. L. SiO_2/Ta_2O_5 Core−Shell Nanowires and Nanotubes. *Angew. Chem., Int. Ed.* **2006**, *45*, 7773–7778.
15. Chueh, Y. L.; Hsieh, C. H.; Chang, M. T.; Chou, L. J.; Lao, C. S.; Song, J. H.; Gan, J. Y.; Wang, Z. L. RuO_2 Nanowires and RuO_2/TiO_2 Core/Shell Nanowires: From Synthesis to Mechanical, Optical, Electrical, and Photoconductive Properties. *Adv. Mater.* **2007**, *19*, 143–149.
16. He, Y. B.; Li, G. R.; Wang, Z. L.; Su, C. Y.; Tong, Y. X. Single-Crystal ZnO Nanorod/Amorphous and Nanoporous Metal Oxide Shell Composites: Controllable Electrochemical Synthesis and Enhanced Supercapacitor Performances. *Energy Environ. Sci.* **2011**, *4*, 1288–1292.
17. Heo, Y. W.; Kaufman, M.; Pruessner, K.; Siebein, K. N.; Norton, D. P.; Ren, F. ZnO/Cubic (Mg,Zn)O Radial Nanowire Heterostructures. *Appl. Phys. A: Mater. Sci. Process.* **2005**, *80*, 263–266.
18. Jung, S.; Yong, K. Fabrication of CuO−ZnO Nanowires on a Stainless Steel Mesh for Highly Efficient Photocatalytic Applications. *Chem. Commun.* **2011**, *47*, 2643–2645.

19. Liu, J. P.; Jiang, J.; Cheng, C. W.; Li, H. X.; Zhang, J. X.; Gong, H.; Fan, H. J. Co_3O_4 Nanowire@MnO_2 Ultrathin Nanosheet Core/Shell Arrays: A New Class of High-Performance Pseudocapacitive Materials. *Adv. Mater.* **2011**, *23*, 2076–2081.
20. Marcu, A.; Yanagida, T.; Nagashima, K.; Oka, K.; Tanaka, H.; Kawai, T. Crucial Role of Interdiffusion on Magnetic Properties of *In-Situ* Formed MgO/Fe_3O_4 Heterostructured Nanowires. *Appl. Phys. Lett.* **2008**, *92*, 173119.
21. Wang, H. W.; Ting, C. F.; Hung, M. K.; Chiou, C. H.; Liu, Y. L.; Liu, Z. W.; Ratinac, K. R.; Ringer, S. P. Three-Dimensional Electrodes for Dye-Sensitized Solar Cells: Synthesis of Indium-Tin-Oxide Nanowire Arrays and ITO/TiO_2 Core–Shell Nanowire Arrays by Electrophoretic Deposition. *Nanotechnology* **2009**, *20*, 055601.
22. Zhao, X. H.; Wang, P.; Li, B. J. CuO/ZnO Core/Shell Heterostructure Nanowire Arrays: Synthesis, Optical Property, and Energy Application. *Chem. Commun.* **2010**, *46*, 6768–6770.
23. Liu, R.; Lee, S. B. MnO_2/Poly(3,4-ethylenedioxythiophene) Coaxial Nanowires by One-Step Coelectrodeposition for Electrochemical Energy Storage. *J. Am. Chem. Soc.* **2008**, *130*, 2942–2943.
24. Cheng, C.; Liu, B.; Yang, H.; Zhou, W.; Sun, L.; Chen, R.; Yu, S. F.; Zhang, J.; Gong, H.; Sun, H.; *et al.* Hierarchical Assembly of ZnO Nanostructures on SnO_2 Backbone Nanowires: Low-Temperature Hydrothermal Preparation and Optical Properties. *ACS Nano* **2009**, *3*, 3069–3076.
25. Cao, L.; Xu, F.; Liang, Y. Y.; Li, H. L. Preparation of the Novel Nanocomposite Co(OH)2/Ultra-stable Y Zeolite and Its Application as a Supercapacitor with High Energy Density. *Adv. Mater.* **2004**, *16*, 1853–1857.
26. Li, Y. G.; Tan, B.; Wu, Y. Y. Mesoporous Co_3O_4 Nanowire Arrays for Lithium Ion Batteries with High Capacity and Rate Capability. *Nano Lett.* **2008**, *8*, 265–270.
27. Li, Y. G.; Tan, B.; Wu, Y. Y. Freestanding Mesoporous Quasi-Single-Crystalline Co_3O_4 Nanowire Arrays. *J. Am. Chem. Soc.* **2006**, *128*, 14258–14259.
28. Mai, L. Q.; Yang, F.; Zhao, Y. L.; Xu, X.; Xu, L.; Luo, Y. Z. Hierarchical $MnMoO_4$/$CoMoO_4$ Heterostructured Nanowires with Enhanced Supercapacitor Performance. *Nat. Commun.* **2011**, *2*, 381.
29. Xia, X. H.; Tu, J. P.; Mai, Y. J.; Wang, X. L.; Gu, C. D.; Zhao, X. B. Self-Supported Hydrothermal Synthesized Hollow Co_3O_4 Nanowire Arrays with High Supercapacitor Capacitance. *J. Mater. Chem.* **2011**, *21*, 9319–9325.
30. Zhao, X.; Sanchez, B. M.; Dobson, P. J.; Grant, P. S. The Role of Nanomaterials in Redox-Based Supercapacitors for Next Generation Energy Storage Devices. *Nanoscale* **2011**, *3*, 839–855.
31. Wei, T. Y.; Chen, C. H.; Chien, H. C.; Lu, S. Y.; Hu, C. C. A Cost-Effective Supercapacitor Material of Ultrahigh Specific Capacitances: Spinel Nickel Cobaltite Aerogels from an Epoxide-Driven Sol–Gel Process. *Adv. Mater.* **2010**, *22*, 347–351.
32. Colfen, H.; Antonietti, M. Mesocrystals: Inorganic Superstructures Made by Highly Parallel Crystallization and Controlled Alignment. *Angew. Chem., Int. Ed.* **2005**, *44*, 5576–5591.
33. Penn, R. L.; Banfield, J. F. Imperfect Oriented Attachment: Dislocation Generation in Defect-Free Nanocrystals. *Science* **1998**, *281*, 969–971.
34. Niederberger, M.; Colfen, H. Oriented Attachment and Mesocrystals: Non-classical Crystallization Mechanisms Based on Nanoparticle Assembly. *Phys. Chem. Chem. Phys.* **2006**, *8*, 3271–3287.
35. Xia, X. H.; Tu, J. P.; Zhang, J.; Wang, X. L.; Zhang, W. K.; Huang, H. Electrochromic Properties of Porous NiO Thin Films Prepared by a Chemical Bath Deposition. *Sol. Energy Mater. Sol. Cells* **2008**, *92*, 628–633.
36. Xia, X. H.; Tu, J. P.; Zhang, Y. Q.; Mai, Y. J.; Wang, X. L.; Gu, C. D.; Zhao, X. B. Freestanding Co_3O_4 Nanowire Array for High Performance Supercapacitors. *RSC Adv.* **2012**, *2*, 1835–1841.
37. Xia, X. H.; Tu, J. P.; Wang, X. L.; Gu, C. D.; Zhao, X. B. Mesoporous Co_3O_4 Monolayer Hollow-Sphere Array as Electrochemical Pseudocapacitor Material. *Chem. Commun.* **2011**, *47*, 5786–5788.
38. Xia, X. H.; Tu, J. P.; Wang, X. L.; Gu, C. D.; Zhao, X. B. Hierarchically Porous NiO Film Grown by Chemical Bath Deposition *via* a Colloidal Crystal Template as an Electrochemical Pseudocapacitor Material. *J. Mater. Chem.* **2011**, *21*, 671–679.
39. Guan, C.; Liu, J. P.; Cheng, C. W.; Li, H. X.; Li, X. L.; Zhou, W. W.; Zhang, H.; Fan, H. J. Hybrid Structure of Cobalt Monoxide Nanowire@Nickel Hydroxidenitrate Nanoflake Aligned on Nickel Foam for High-Rate Supercapacitor. *Energy Environ. Sci* **2011**, *4*, 4496–4499.
40. Liu, J. P.; Cheng, C. W.; Zhou, W. W.; Li, H. X.; Fan, H. J. Ultrathin Nickel Hydroxidenitrate Nanoflakes Branched on Nanowire Arrays for High-Rate Pseudocapacitive Energy Storage. *Chem. Commun.* **2011**, *47*, 3436–3438.